Turkish Journal of Electrical Engineering and Computer Sciences

Volume 24 | Number 4 Article 34

1-1-2016

Fetal electrocardiogram estimation using polynomial eigenvalue decomposition

SOYDAN REDIF

Turkish Journal of Electrical Engineering & Computer Sciences

http://journals.tubitak.gov.tr/elektrik/

Research Article

Turk J Elec Eng & Comp Sci
(2016) 24: 2483 – 2497

doi:10.3906/elk-1401-19

Fetal electrocardiogram estimation using polynomial eigenvalue decomposition

Soydan REDIF*
Department of Electrical and Electronic Engineering, Faculty of Engineering, European University of Lefke, Gemikonağı-Lefke, Northern Cyprus

Received: 02.01.2014 • **Accepted/Published Online:** 19.08.2014 • **Final Version:** 15.04.2016

Abstract: In this paper, we propose the application of polynomial matrix eigenvalue decomposition (PEVD) to the problem of fetal electrocardiogram (ECG) extraction from real ECG recordings obtained from abdominal leads. We model the fetal ECG extraction problem as a broadband sensor array signal processing problem in order to account for the broadband nature of the ECG noise present in the recordings. An algorithm for providing an approximate PEVD is used in order to estimate the broadband noise subspace. Suppression of the broadband noise and maternal ECG is achieved by carrying out an orthonormal projection of the recordings onto the estimated fetal subspace. The proposed scheme was evaluated with multichannel synthetic ECG signals and real ECG data from the PhysioNet Challenge database and is shown to perform favorably as compared to prior-art methods. Results indicate that our method is more robust than the prior-art ones for the task of fetal ECG estimation.

Key words: Fetal electrocardiogram extraction, polynomial matrix eigenvalue decomposition, broadband subspace decomposition

1. Introduction

The accurate estimation of the QRS complexes of fetal electrocardiogram (FECG) waveforms is an essential part of prenatal diagnosis of fetal heart conditions [1]. The antepartum FECG can be measured noninvasively from electrodes on the mother's skin. However, FECG signals are very weak compared to the background interference, the strongest of which is the maternal ECG (MECG) signal. Other noise sources, such as uterine electromyographic noise, baseline wander, and muscle noise, also cause problems [2]. As a consequence, the estimation of the FECG has remained an open problem.

The FECG extraction problem has been addressed in the past using various methods, such as neural networks [3,4], Bayesian inference [5], adaptive filtering [6 – 8], and blind source separation (BSS) [8 – 13]. Sameni et al. proposed a method based on both periodic independent component analysis (ICA) and generalized eigenvalue decomposition, namely the periodic ICA (PiCA) algorithm, in [11]. It is known that if the FECG signal power across all the channels is significantly less than that of the MECG, then decorrelation alone, via principal component analysis (PCA) or singular-value decomposition (SVD) [12], can usually separate the signals from the noise [13 – 16]. A drawback of this approach is that its performance depends on the electrode positioning [15].

The muscle, observation, and quantization noises [10,13,17 – 19] picked up by the sensors have significant

*Correspondence: sredif@eul.edu.tr

frequency extent (broadband), so they cannot be adequately related in terms of simple phase and amplitude factors across the sensors. The consideration of only instantaneous correlation is suboptimal if not entirely inappropriate; therefore, decorrelation over all relative time delays, i.e. strong decorrelation [20], is necessary. Strong decorrelation can be imposed by application of a matrix of suitably chosen finite impulse response (FIR) filters, or a polynomial matrix [21]. The required polynomial matrix is obtained via a polynomial matrix eigenvalue decomposition (PEVD), which has received growing interest recently [22 – 27]. In [23], McWhirter et al. proposed the second-order sequential best rotation (SBR2) algorithm. In [26], the authors introduced a new variant of SBR2 modified for subband coding, namely SBR2C, which was shown to give improved performances.

In this paper, a novel approach to FECG signal extraction and fetal R-wave estimation is proposed that uses the SBR2C algorithm of [26] for computing the PEVD of the cutaneous recordings, for which only initial results were obtained using the SBR2 of [27]. PEVD enables the estimation of the broadband noise subspace and maternal and fetal signal subspaces, from which the fetal R-waves are estimated.

1.1. Problem statement

The broadband noise contributions in the ECG recordings originate from sources that typically have colored spectra and thus long-term correlations [17 – 19], which, if long enough, could mean that the coherence time becomes large compared to the source waveforms. Consequently, the sampled sensor signals may look as if they have been through a time-dispersive channel. In addition, the impinging signals may not be coherent across the different sensors, i.e. weak correlation between sensor signals, which can be problematic for multichannel BSS algorithms. We account for the lag-dependent correlations by modeling the source-to-sensor propagation as a matrix of FIR filters, rather than a scalar matrix, akin to broadband array processing. The transfer function of the FIR matrix forms a polynomial matrix, which accurately describes (matches) the possibly fractional [28] pure delays between different sensors, as described in this section.

1.2. Preliminary

A matrix $\mathbf{R}$ is a Hermitian matrix if $\mathbf{R} = \mathbf{R}^H$ and a unitary matrix $\mathbf{H} \in C^{p\times p}$ is one that satisfies $\mathbf{H}^H\mathbf{H} = \mathbf{I}_p$, where $\mathbf{I}_p$ is the $p \times p$ identity matrix. A polynomial matrix is a polynomial with matrix coefficients. A $p \times q$ polynomial matrix in the indeterminate z^{-1} is denoted by

$$\underline{\mathbf{A}}(z) = \sum_{\tau=t_1}^{t_2} \mathbf{A}[\tau] z^{-\tau}, \tag{1}$$

where $\tau \in Z$, $t_1 \leq t_2$. Here we use the underscore notation to denote a polynomial (and Laurent polynomials) or power series. The matrix $\underline{\mathbf{A}}(z)$ has entries $\underline{a}_{ik}(z) = \sum_{\tau=t_1}^{t_2} a_{ik}[\tau] z^{-\tau}$ with $a_{ik}[\tau] \in C\, \forall ik\tau$. A transform pair in Eq. (1) is denoted as $\underline{\mathbf{A}}(z) \leftrightarrow \mathbf{A}[\tau]$. The matrices $\mathbf{A}[t_1], \ldots, \mathbf{A}[t_2]$ are referred to as the coefficient matrices of $\underline{\mathbf{A}}(z)$; e.g., $\mathbf{A}[0]$ is the coefficient matrix (plane) of order zero, i.e. coefficient matrix at z^0.

A polynomial matrix $\underline{\mathbf{H}}(z)$ is paraunitary (PU) if the matrix $\underline{\mathbf{H}}(z)|_{z=e^{j\Omega}} = \mathbf{H}\left(e^{j\Omega}\right) \in C^{p\times p}$ is unitary for all frequencies Ω. Equivalently, $\underline{\mathbf{H}}(z)\tilde{\underline{\mathbf{H}}}(z) = \tilde{\underline{\mathbf{H}}}(z)\underline{\mathbf{H}}(z) = \mathbf{I}_p$, where $\tilde{\underline{\mathbf{H}}}(z)$ is the paraconjugate transpose of $\underline{\mathbf{H}}(z)$, i.e. $\underline{\mathbf{H}}^H(1/z^*)$. In the context of linear system theory, $\underline{\mathbf{H}}(z)$ represents a lossless multiinput multioutput transfer function [29]. The matrix $\underline{\mathbf{R}}(z) \in \underline{C}^{p\times p}$ is para-Hermitian if $\tilde{\underline{\mathbf{R}}}(z) = \underline{\mathbf{R}}(z)$; so $\{\mathbf{R}[\tau]\}_{ik} = r_{ik}[\tau] = r^*_{ki}[-\tau] = \{\mathbf{R}[-\tau]\}^*_{ki}$, $\forall \tau \in Z$ and $ik = 1, 2 \ldots p$.

1.3. Data model

Consider that q signals, $\mathbf{s}[t] \in R^q$, from statistically independent sources, are received by p cutaneous sensors producing the signals $\mathbf{x}[t] \in R^p$, where $p \geq q$. Since some source signals consist of an infinite number of different frequency components, the sensor-weight values required to correct for the possibly fractional [28] time delay between sensors are different for different frequencies. Frequency-dependent weights can be realized using FIR filters, which form a frequency-dependent response for each sensor signal in order to compensate the phase difference for the different frequency components. The sensors thus sample the propagating wave field in both space and time. This processing can be expressed as

$$\mathbf{x}[t] = \sum_{\tau=t_1}^{t_2} \mathbf{A}[\tau]\,\mathbf{s}[t-\tau] + \eta[t] \tag{2}$$

where $\mathbf{A}[t] \in R^{p\times q}$ is the matrix of (unknown) FIR filter coefficients $a_{ik}[t]$, which corrupt the sources. The mixing matrix $\mathbf{A}[t]$ is defined by the geometry of the body and sensor and the source positions. $\eta[t]$ represents the additive noise, which is independent from the source signals. Eq. (2) may also be written as:

$$\underline{\mathbf{x}}(z) = \underline{\mathbf{A}}(z)\,\underline{\mathbf{s}}(z) + \underline{\eta}(z) \tag{3}$$

where $\underline{\mathbf{x}}(z)$, $\underline{\mathbf{s}}(z)$ and $\underline{\eta}(z)$ denote power series of the form $\underline{\mathbf{x}}(z) = \sum_{t=-\infty}^{\infty} \mathbf{x}[t]\,z^{-t}$.

Due to the process in Eq. (2), the signals $\underline{\mathbf{x}}(z)$ will generally be correlated over multiple time lags. Accordingly, the space-time covariance matrix, which is para-Hermitian,

$$\mathbf{R}[\tau] = E\left\{\mathbf{x}[t]\,\mathbf{x}^H[t-\tau]\right\} \tag{4}$$

will generally not be diagonal, where $E\{\cdot\}$ denotes the expectation operator. It follows that the cross-spectral density (CSD) matrix $\underline{\mathbf{R}}(z) \leftrightarrow \mathbf{R}[\tau]$,

$$\underline{\mathbf{R}}(z) = \underline{\mathbf{A}}(z)\,\underline{\mathbf{R}}_{\mathbf{ss}}(z)\,\tilde{\underline{\mathbf{A}}}(z) + \underline{\mathbf{R}}_{\eta\eta}(z) \tag{5}$$

will also not be diagonal. $\underline{\mathbf{R}}_{\mathbf{ss}}(z)$ and $\underline{\mathbf{R}}_{\eta\eta}(z)$ are the CSD matrices of the q sources and p noise sources, respectively, and are both diagonal because of the independence assumption.

2. Eigenvalue decomposition of para-Hermitian systems

In order to gain an estimate of the FECG subspace, the diagonalization of $\underline{\mathbf{R}}(z)$ is required. In this section, we provide a brief review of the PEVD and an algorithm for computing the PEVD, which is central to the proposed method described in Section 3.

2.1. Polynomial matrix eigenvalue decomposition

The signals $\mathbf{x}[t]$ cannot be expressed in terms of simple amplitude and phase factors because they represent broadband sensor signals. Usually, decorrelation by the SVD (or EVD) [12] is not adequate, so we are often required to perform strong decorrelation:

$$E\left\{\sum_t x_i[t]\,x_k[t+\tau]\right\} = 0,\ \forall\tau,\ i \neq k \tag{6}$$

It turns out that to satisfy Eq. (6) we require a PU matrix $\underline{\mathbf{H}}(z) \leftrightarrow \mathbf{H}[\tau]$, such that the transformed signal vector,

$$\mathbf{w}[t] = \sum_{\tau=-\infty}^{\infty} \mathbf{H}[\tau]\,\mathbf{x}[t-\tau] \tag{7}$$

is strongly decorrelated [23]. This requires that the CSD matrix, $\underline{\mathbf{S}}(z)$, of the transformed signals $\mathbf{w}[t] \in C^p$ be diagonalized, i.e.

$$\underline{\mathbf{S}}(z) = \underline{\mathbf{H}}(z)\,\underline{\mathbf{R}}(z)\,\tilde{\underline{\mathbf{H}}}(z) = \mathrm{diag}\left\{\underline{s}_{11}(z) \ldots \underline{s}_{pp}(z)\right\} \tag{8}$$

where $\underline{\mathbf{S}}(z) \leftrightarrow \mathbf{S}[\tau]$ is the covariance matrix $\mathbf{S}[\tau] = E\{\mathbf{w}[t]\,\mathbf{w}^H[t-\tau]$ of the transformed signals and $\mathrm{diag}\{\bullet\}$ denotes a diagonal matrix. The diagonal elements $\underline{s}_{kk}(z)$ are the polynomial eigenvalues of $\underline{\mathbf{R}}(z)$, which have the spectral majorization property [20], i.e. the power spectral densities (PSDs) $\underline{\mathbf{S}}(z)|_{z=e^{j\Omega}} = \mathbf{S}\left(e^{j\Omega}\right) \in C^{p\times p}$ satisfy

$$S_{11}\left(e^{j\Omega}\right) \geq \ldots \geq S_{pp}\left(e^{j\Omega}\right) \quad \forall\Omega. \tag{9}$$

Eqs. (8) and (9) give an extension of the 'ordered' EVD to polynomial matrices, which is referred to as polynomial matrix EVD (or PEVD). Note that Eqs. (6) and (8) are equivalent statements in the sense that the transformed signals, which satisfy Eq. (6), correspond to the diagonals of $\underline{\mathbf{S}}(z)$. Also note that since $\underline{\mathbf{H}}(z)$ is PU, $\|\underline{\mathbf{R}}(z)\|_F = \|\underline{\mathbf{S}}(z)\|_F$, where $\|.\|_F$ denotes the Frobenius norm. Eq. (9) may be viewed as analogous to the ordering of the singular values by the SVD. If there is sufficient disparity in the powers of the broadband source signals, then BSS may be achieved via the PEVD.

2.2. SBR2C algorithm

The SBR2 algorithm is an iterative, time-domain algorithm based on second-order statistics [23]. It generalizes the classical Jacobi method to para-Hermitian polynomial matrices. The enhanced variant of SBR2 in [26], namely the coding gain-based SBR2 (SBR2C), maximizes the coding gain function in [20] and gives improved strong decorrelation and spectral majorization. Here we give a very short review of SBR2C as it forms the basis of the proposed scheme in Section 3. Readers are referred to [26] for a thorough treatment of SBR2C.

The SBR2C algorithm computes an FIR PU matrix $\underline{\mathbf{H}}(z)$ such that Eqs. (8) and (9) are satisfied to a good approximation. The SBR2C algorithm can attain an approximate factorization of the form

$$\underline{\mathbf{S}}_L(z) = \underline{\mathbf{H}}_L(z)\,\hat{\underline{\mathbf{R}}}(z)\,\tilde{\underline{\mathbf{H}}}_L(z) \approx \mathrm{diag}\left\{\underline{s}_{L,11}(z) \ldots \underline{s}_{L,pp}(z)\right\} \tag{10}$$

after L iterations. $\hat{\underline{\mathbf{R}}}(z)$ is an estimate of $\underline{\mathbf{R}}(z)$ based on samples from $\underline{\mathbf{x}}(z)$ in Eq. (3); $\underline{\mathbf{S}}_L(z)$ is a good approximation to the diagonalized $\underline{\mathbf{S}}(z)$ of Eq. (8). At each iteration l, SBR2C eliminates the largest normalized magnitude-square off-diagonal term,

$$g = \frac{|s_{L-1,m,n}[\tau]|^2}{s_{L-1,m,m}[0]\,s_{L-1,n,n}[0]}, \tag{11}$$

of $\underline{\mathbf{S}}_{l-1}(z)$, where $s_{l-1,m,m}[0]$ and $s_{l-1,n,n}[0]$ are variance of the mth and nth signals, respectively. The matrix $\underline{\mathbf{S}}_L(z)$ is adequately diagonalized after L iterations, so that

$$\max_{m,n,m\neq n,\tau} g \leq \epsilon, \tag{12}$$

where ϵ is a predesignated arbitrarily small threshold parameter; and the polynomial matrices $\underline{\mathbf{S}}_L(z)$ and $\underline{\mathbf{H}}_L(z)$ are as in Eq. (10). The PU matrix is obtained thus as

$$\underline{\mathbf{H}}_L(z) = \left(\prod_{l=L}^{1} \underline{\mathbf{P}}_l(z)\right) \tag{13}$$

whereby the *elementary* PU matrix $\underline{\mathbf{P}}_l(z) = \mathbf{U}_l \underline{\mathbf{\Lambda}}_l(z)$ consists of a Jacobi rotation matrix $\mathbf{U}_l$ and a PU (delay) matrix $\underline{\mathbf{\Lambda}}_l(z)$ [23]. For each l, an elementary PU matrix transfers energy from the off-diagonals of $\underline{\mathbf{S}}_{l-1}[\tau_l]$ to its diagonals such that the larger diagonal element of the order-zero coefficient matrix, $\mathbf{S}_{l-1}[0]$, lies higher up on the diagonal, which during the iteration process leads to spectral majorization.

The accuracy of this decomposition depends on ϵ, the support of $\hat{\underline{\mathbf{R}}}(z)$ and the method used to estimate $\underline{\mathbf{R}}(z)$—-a procedure for calculating $\hat{\underline{\mathbf{R}}}(z)$ is given in Section 3. Note that the order of $\underline{\mathbf{H}}(z)$ cannot be determined prior to applying SBR2C, which is in contrast to other methods (e.g., [25]), which design degree-constrained PU matrices.

3. Proposed method for fetal ECG extraction

In this section, we describe a method that uses the SBR2C algorithm for estimating the FECG signal from multichannel abdominal ECG recordings. The proposed method is an extension of the methodology reported in [27], which used SBR2. The decomposition in Eq. (10) allows an estimate of the fetal subspace; projection of the data onto this subspace produces estimates of the FECG, as discussed in the following section.

3.1. CSD matrix estimation

All current PEVD approximating algorithms, including SBR2C, are blind techniques in the sense that they do not have prior knowledge of the sources or the mixing matrix, only necessitating knowledge of the space-time covariance matrix $\mathbf{R}[\tau]$ in Eq. (5). For real-life applications, we calculate an estimate of $\underline{\mathbf{R}}(z)$, using T samples, say, of the input $\mathbf{x}[t]$, i.e.

$$\hat{\underline{\mathbf{R}}}(z) \triangleq \sum_{\tau=-W}^{W} \hat{\mathbf{R}}[\tau] z^{-\tau} \tag{14}$$

where

$$\hat{\mathbf{R}}[\tau] \triangleq \frac{1}{T} \sum_{t=0}^{T-1} \mathbf{x}[t] \mathbf{x}^H[t-\tau], \quad \tau \in Z, \quad 0 \leq t \leq T-1 \tag{15}$$

It is assumed that the signals $\mathbf{x}[t]$ have zero mean, $T \gg W$ and $\hat{R}[\tau] \cong 0$, for $|\tau| > W$, where $2W+1$ is the window length [23], so for broadband signals, $\hat{R}[\tau]$ is negligibly small if $|\tau|$ is large compared to the coherence time. The parameter W is often measured empirically; $\mathbf{x}[t] = 0$ for t outside the interval $[0, T-1]$.

3.2. Application of the SBR2C algorithm

SBR2C (in Section 2) is used to strongly decorrelate the ECG signals $\mathbf{x}[t]$ derived from the electrodes placed on the patient. The algorithm generates a PU matrix $\mathbf{H}(z)$ s.t.

$$\underline{\mathbf{H}}(z) \hat{\underline{\mathbf{R}}}(z) \tilde{\underline{\mathbf{H}}}(z) = \hat{\underline{\mathbf{S}}}(z) \tag{16}$$

where $\hat{S}(z)$ is approximately diagonal; more specifically,

$$\hat{\underline{\mathbf{S}}}(z) \approx \operatorname{diag}\left\{\hat{\underline{s}}_1(z), \hat{\underline{s}}_2(z), \ldots, \hat{\underline{s}}_p(z)\right\} \tag{17}$$

The lossless filter represented by $\underline{\mathbf{H}}(z)$ is then applied to the input signals $\mathbf{x}[t]$ to produce the transformed signals according to Eq. (7), or

$$\underline{\mathbf{w}}(z) = \underline{\mathbf{H}}(z)\,\underline{\mathbf{x}}(z) \tag{18}$$

where the signals $\underline{\mathbf{w}}(z)$ and $\underline{\mathbf{x}}(z)$ are algebraic power series. To a good approximation, the signals $\underline{\mathbf{w}}(z)$ are strongly decorrelated and spectrally majorized for multichannel data [23]. The transformed signals $\underline{\mathbf{w}}(z)$ have signal contributions from the FECG, MECG, and noise signals and can be viewed as the *polynomial principal* components of $\underline{\mathbf{x}}(z)$.

3.3. Proposed method

A salient feature of SBR2C is its very strong tendency to produce spectrally majorized signals, thereby compacting the maximum power into the least number of channels [26]. This enables it to be used for estimating broadband signal and noise subspaces with the aim of performing a degree of BSS. Typically the power of the MECG is sufficiently large enough compared to that of the FECG in the recordings so as to partition the approximated CSD matrix, $\hat{\underline{\mathbf{S}}}(z)$, corresponding to $\underline{\mathbf{w}}(z)$, as:

$$\hat{\underline{\mathbf{S}}}(z) \approx \operatorname{diag}\left\{\hat{\underline{s}}_1(z), \hat{\underline{s}}_2(z), \hat{\underline{\mathbf{S}}}_\eta(z)\right\} \tag{19}$$

where $\hat{\underline{s}}_1(z)$ is an estimate of the polynomial eigenvalue associated with the MECG. If the FECG signal is strong compared to the noise sources, then $\hat{\underline{s}}_2(z)$ is the polynomial eigenvalue associated with the FECG and corresponds to an estimate of the fetal subspace; $\hat{\underline{\mathbf{S}}}_\eta(z) \triangleq \operatorname{diag}\left\{\hat{\underline{s}}_3(z), \ldots, \hat{\underline{s}}_p(z)\right\}$ is associated with sources of noise. The polynomial eigenvectors of $\hat{\underline{\mathbf{R}}}(z)$ constitute the columns of $\underline{\mathbf{H}}(z)$ which span $\underline{\mathbf{x}}(z)$. The noise power usually dominates a very weak FECG signal, in which case the ordering of the polynomial eigenvalues in Eq. (19) can be different. This may occur since SBR2C has a strong tendency to compact the most powerful correlated components into $\underline{w}_1(z)$, and the next most powerful into $\underline{w}_2(z)$, and so on [26].

It is assumed that the three subspaces relating to $\hat{\underline{s}}_1(z)$, $\hat{\underline{s}}_2(z)$ and $\hat{\underline{\mathbf{S}}}_\eta(z)$ are orthogonal. FECG estimation is achieved by orthonormal projection of the data onto the fetal subspace, namely back projection, given by

$$\hat{\underline{f}}(z) = \tilde{\underline{\mathbf{H}}}(z)\,\mathbf{B}\underline{\mathbf{w}}(z) \tag{20}$$

where $\mathbf{B} \in Z^{p\times p}$, called the *blocking matrix*, is a diagonal matrix with the diagonal corresponding to the FECG component set to unity. For example, in the case of Eq. (19),

$$\mathbf{B} = \operatorname{diag}\left\{0\ 1\ \underbrace{0\ \ldots\ 0}_{p-2}\right\} \tag{21}$$

Eq. (20) is depicted in Figure 1. The p signals in $\hat{\underline{f}}(z)$ are estimates of the FECG, $\underline{f}(z)$. Conversely, for an MECG estimate, the maternal component is back projected using $\mathbf{B} = \operatorname{diag}\{1\ \underbrace{0\ \ldots\ 0}_{p-1}\}$ in Eq. (20).

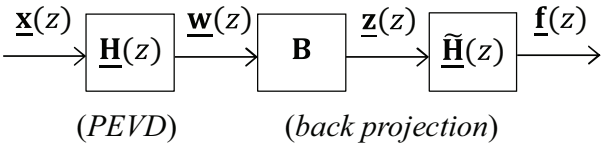

Figure 1. The proposed scheme for FECG extraction.

In practice, the correct choice of the blocking matrix $\mathbf{B}$ in Eq. (20) can be made by visually inspecting the transformed signals $\underline{\mathbf{w}}(z)$—the signal with recurring fetal R-wave components and minimal MECG remnants is used in Eq. (20). This process can be automated by finding the set $\{\underline{\omega}_k(z)\}$ in $\underline{\mathbf{w}}(z)$ whose members have a strong correlation with a reference of the maternal ECG, $\underline{m}(z)$. The reference $\underline{m}(z)$ can be obtained from a thoracic sensor. Correlations between $\underline{\mathbf{w}}(z)$ and $\underline{m}(z)$ are computed, and the signals $\underline{\omega}_k(z)$ with correlations above a preselected threshold $\zeta \in (0,1]$ are then omitted from Eq. (20). The indices k define the locations of the zeros on the diagonal of $\mathbf{B}$. The accuracy of this detection process depends on ζ and the estimated cross-correlation between $\underline{\mathbf{w}}(z)$ and $\underline{m}(z)$. A suitable value of ζ is found experimentally. In situations where all in $\underline{\mathbf{w}}(z)$ are highly correlated with $\underline{m}(z)$, the algorithm defaults to that in Eq. (21).

4. Results and discussion

In this section, a study of the performance of the proposed method for fetal ECG extraction is presented for both synthetic abdominal ECG signals and real-world ECG recordings. Our method is compared to three other multichannel algorithms for FECG estimation.

4.1. Experiments using synthetic ECG signals

The synthetic ECG data used in this paper are the 3-D, multichannel, dynamic model in [17] for body surface ECG recordings, where the heart beat rate and noise level can be varied. In our simulations, different MECG, FECG, and noise signals were synthesized. To improve the simulation realism, real muscle artifact, baseline wander, and motion artifacts from the MIT-BIH Noise Stress Test Database [30,31] were used. This database includes 3 half-hour recordings of noise typical in ambulatory ECG recordings. The data were anti-aliased resampled from an original sampling frequency of 360 Hz to match that of the ECG signals (500 Hz); resampling had minimal effect on the noise structure.

The signal-to-noise ratio (SNR) and signal-to-interference ratio (SIR) of the FECG signal were adjusted with the noise and maternal signal power levels, respectively. The simulated maternal, fetal, noise, and synthetic abdominal signals are shown in Figures 2a–2d, respectively. Corresponding spectra of these signals are shown in Figures 2e–2h. The signals were simulated with an input SNR and SIR of -15 dB.

The SBR2C algorithm was applied to three synthetic abdominal ECG channels of the type in Figure 2d. The convergence of SBR2C for different values of the parameter W in Eq. (14) is shown by the graph of g from Eq. (11) versus iteration number L in Figure 3. We see that SBR2C achieves lower values of g for $W = 20$. SBR2C is seen to converge faster, in general, than the (original) SBR2 algorithm, whose convergence for $W = 20$ is also included in Figure 3. The correct choice of W depends on the main lobe of the correlation lag-extent of the ECG signals. Studies of these correlations for both synthetic and real ECG signals have shown that, generally, $W = 20$ gives the best results, since the main lobe of the ECG correlations have a mean extent of ~ 40 samples with a standard deviation of 9%. In the following text, the proposed method uses SBR2C with $L = 125$, which yielded $g < 10^{-4}$.

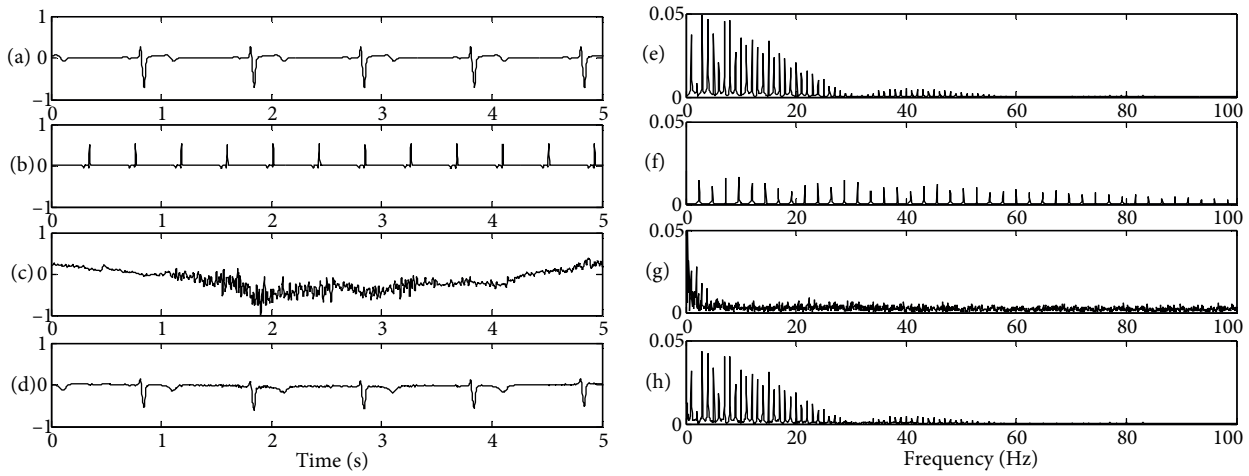

Figure 2. Components of a single synthetic ECG signal: a) MECG signal with a heart rate of 61 bpm, b) FECG signal with a heart rate of 149 bpm, c) real noise signal, and d) synthetic abdominal signal with $SNR = SIR = -15$ dB; e–h) spectra of the MECG, FECG, noise, and abdominal signals.

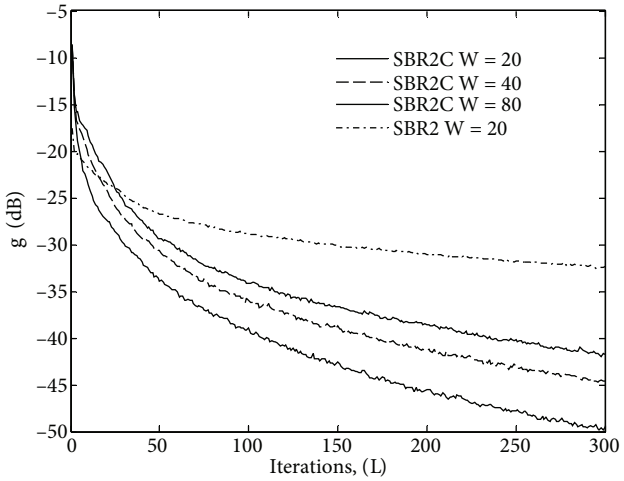

Figure 3. Convergence of SBR2C for W values in the case of 3 synthetic abdominal signals of the type in Figure 2d.

The proposed scheme was applied to the three synthetic abdominal ECG signals. Figures 4a–4c show the principal components $\underline{\mathbf{w}}(z)$ in Eq. (18) produced by SBR2C for the synthetic ECG in Figure 2. On inspection, the 2nd component (2nd graph down from the top) looks to be a reasonable estimate of the fetal subspace since the R-wave periodicity approximates that of the actual FECG in Figure 2b. The principal-component spectra $\underline{\mathbf{w}}(z)|_{z=e^{j\Omega}} = \mathbf{w}\left(e^{j\Omega}\right)$ are shown in Figures 4d–4f. Notice that SBR2C has performed energy compaction (i.e. it has transferred most energy into as few channels as possible) and the first output channel has most of the power, which is mostly due to the maternal ECG.

Back projection of the 2nd output from $\underline{\mathbf{w}}(z)$ onto the ECG inputs using the blocking matrix in Eq. (21) produces the FECG estimates shown in Figure 5. The first output in Figure 5a can be considered a reasonable estimate of the actual FECG signal (in Figure 2b), with a signal-to-interference plus noise ratio (SINR) of 6.4

dB. We define the SINR as

$$SINR = \frac{\|f(t)\|_F^2}{\left\|\hat{\underline{\mathbf{f}}}(t) - f(t)\right\|_F^2} \tag{22}$$

where $f(t)$ is the actual fetal ECG component and $\|f(t)\|_F$ is its Frobenius norm.

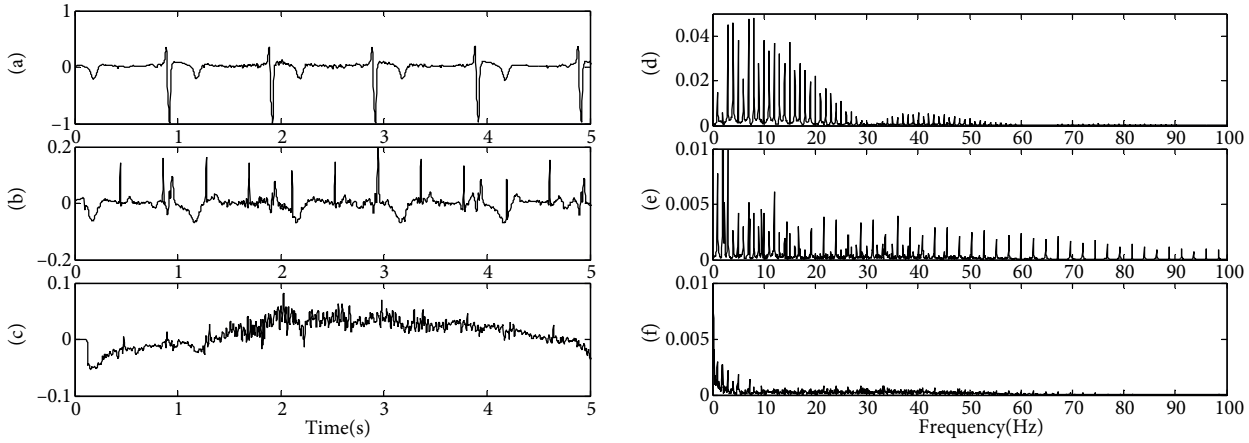

Figure 4. Outputs from the proposed algorithm from processing synthetic abdominal ECG data: a–c) principal components, $\underline{\mathbf{w}}(z)$ from Eq. (18); d–f) spectra of $\underline{\mathbf{w}}(z)$.

The SINR performance of our method was assessed for different noise power levels using three synthetic ECG channels. The input SNR was varied from -10 dB to -24 dB in steps of 2 dB, with $SIR = 0$ dB. For each SNR, the SINR for the estimated FECG signal was calculated as an average over 150 independent experiments. The correlation-based technique described in Section 3.3 was employed; the 1st ECG signal was used as a reference with $\zeta = 0.65$. Figure 6 shows the ensemble average SINR versus SNR.

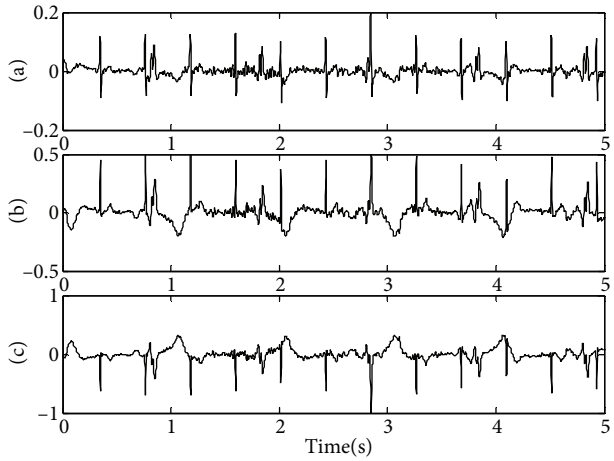

Figure 5. Simulation results from applying the proposed method to three synthetic abdominal signals.

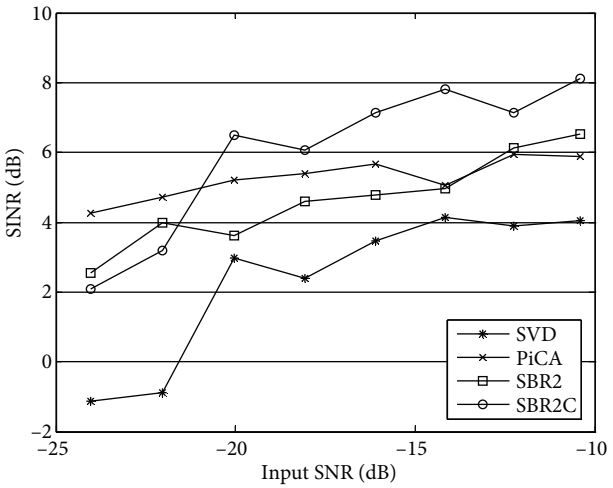

Figure 6. Ensemble SINR of the estimated FECG versus input SNR for four FECG extraction methods.

The performances of three other multichannel methods for FECG estimation are included in Figure 6. The methods evaluated are: 1) the well-known SVD-based method [15]; 2) the periodic component analysis

(PiCA) algorithm [11]; 3) the method based on SBR2 in [27]. Both the SVD- and SBR2-based methods were applied as described in [15] and [27], respectively, where the 2nd transformed component is used in the orthonormal projection. The PiCA method was employed with FECG-beat synchronization, where the best fetal ECG component extracted by the JADE algorithm [14], a BSS method, was used for fetal R-peak detection and phase calculation, as suggested in [11]. Figure 6 illustrates the robustness of our method compared to the other methods for $SNR > -19\,dB$.

4.2. Experiments using Real ECG Recordings

We have also performed experiments on real-world ECG data from the noninvasive fetal ECG PhysioNet Challenge 2013 database [30,32]. This database contains 175 four-channel abdominal FECG recordings over durations of $60\,s$, 10 min, and 60 min from multiple subjects using a variety of instrumentations with differing frequency responses. A sampling frequency of 1 kHz and 12-bit resolution were used. The database included datasets Set-A and Set-B. The former is provided with reference annotations, which were used to check the validity of our results, whereas reference annotations are not available for the latter dataset. The database presents a difficult problem for BSS algorithms due to powerful broadband noise, which varies between datasets.

According to the current limited understanding of FECG processing, FECG estimates should satisfy at least two criteria [7]: 1) the recurring fetal R-waves should be distinctly visible; and 2) there should be no visible remnants of the MECG component. As such, our method obtains good estimates of the FECG for $\sim 71\,\%$ of the PhysioNet Challenge 2013. The Table shows the R-wave detection success rate of the proposed method for Set-A of the Challenge 2013 database. For comparison, we include the performance of the considered prior-art algorithms: PCA (via SVD) [15], PiCA (via JADE) [11], and SBR2 [27]. Note that the first output of the algorithms was used in determining algorithm success.

Table. Comparison of the average R-wave detection performances for Set-A.

Method	**Success rate (%)**
PCA [15]	41.13
PiCA [11]	63.91
SBR2-based [27]	65.85
Proposed method	71.64

The four-channel abdominal ECG recordings for three 10 s examples obtained from the PhysioNet database are shown in Figures 7–9. Note that amplitude values are normalized. Figures 7–9 show segments of the "a15", "a40", and "b08" ECG recordings, respectively. Notice the baseline wander, due to maternal respiration, in Figures 7 and 8, and the very strong maternal signal present in Figure 9. Dataset "a40" is a somewhat pathological example due to the structured noise.

The proposed method was set up as described in Section 4.1. Figure 10a shows the outputs $\underline{\mathbf{w}}(z)$ of Eq. (18) from SBR2C for the recordings in Figure 7. Note that longer recordings (10 min and 60 min) have been analyzed using our method with similar outcomes. On inspection, the 4th component (from the top) is a reasonable estimate of the fetal subspace. For most other datasets, however, the 2nd output channel from SBR2C was dominated by the fetal component. Reasons for this behavior are given in Section 3.3. The corresponding spectra, $\mathbf{w}\left(e^{j\Omega}\right)$, are shown in Figure 10b. Notice that SBR2C has performed energy compaction with the maternal ECG dominating the 1st output.

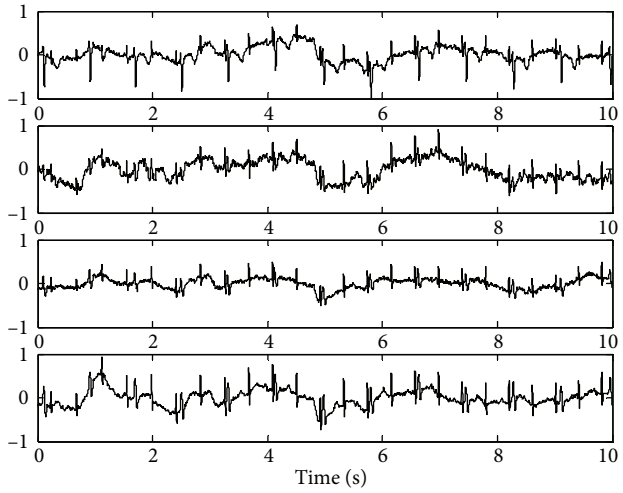

Figure 7. Four abdominal ECG recordings from the "a15" dataset (Set-A) of the ECG Challenge 2013 PhysioNet Database.

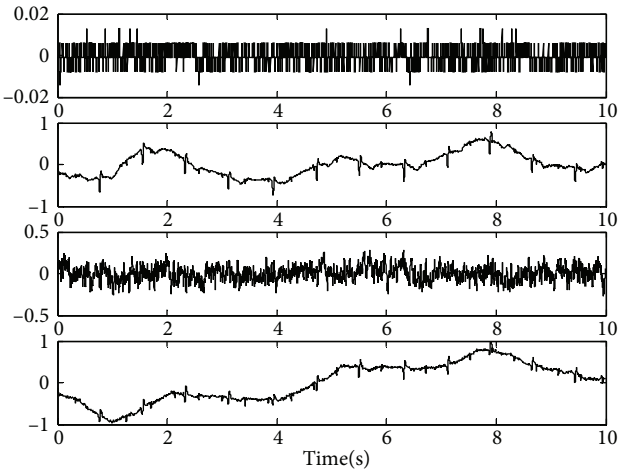

Figure 8. Pathological example of four abdominal ECG recordings from the "a40" dataset (Set-A) of the ECG Challenge 2013 PhysioNet Database. Notice that the first channel has much distortion.

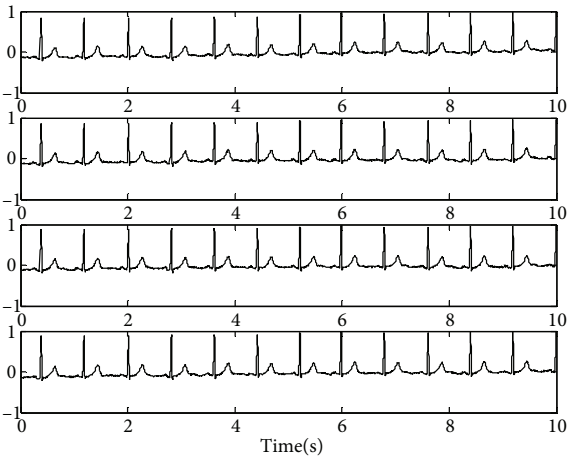

Figure 9. Four abdominal ECG recordings from the "b08" dataset (Set-B) of the ECG Challenge 2013 PhysioNet Database.

Estimates of the FECG are obtained by back projecting the 4th signal, shown in Figure 11a. It can be seen that the first two output signals are fairly clear estimates of the FECG, as verified by the ground truth. Outputs 3 and 4 also have fetal cardiac contributions, but are corrupted by, possibly, baseline wander. The corresponding frequency spectra are shown in Figure 11b. The fetal P- and T-waves are mainly low-frequency components (25 Hz), whereas the fetal QRS complex is localized at higher frequencies ($>$20 Hz). From Figure 11b, we see harmonics relating to a fetal ECG; however, notice that there is little low-frequency content, which suggests that the P- and T-wave components have been suppressed.

For comparison, the PiCA algorithm was also applied to these data, and the results are shown in Figure 12. Figure 12a shows the estimated FECG component (2nd from the top), in which the fetal contributions are clearly visible. Notice that low-frequency components ($<$10 Hz) of the abdominal signal are preserved, which may have more to do with baseline wander than the fetal P- and T-waves.

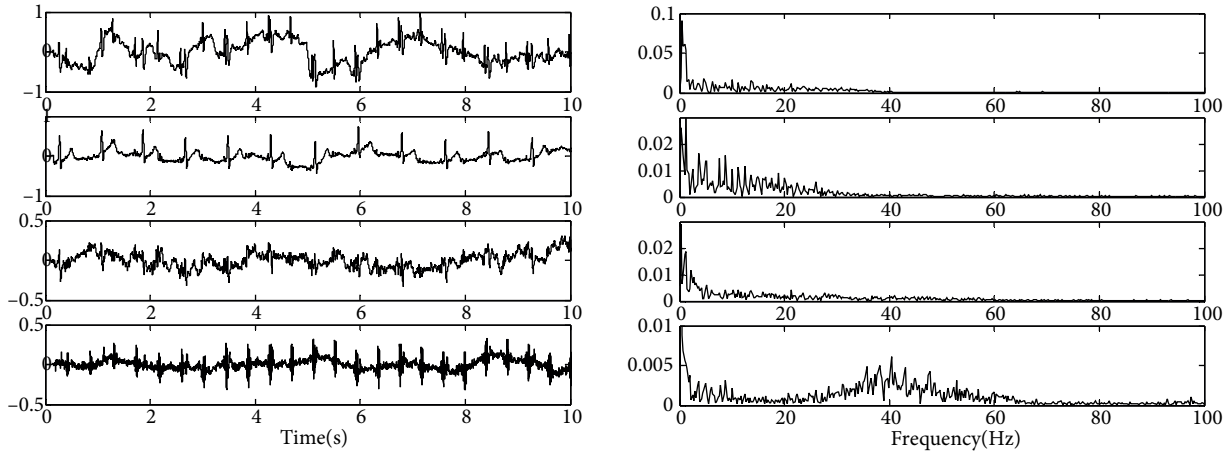

Figure 10. a) Principal components, $\underline{\mathbf{w}}(z)$, extracted from the abdominal ECG dataset "a15" of Figure 7 using the proposed algorithm; b) spectra of $\underline{\mathbf{w}}(z)$.

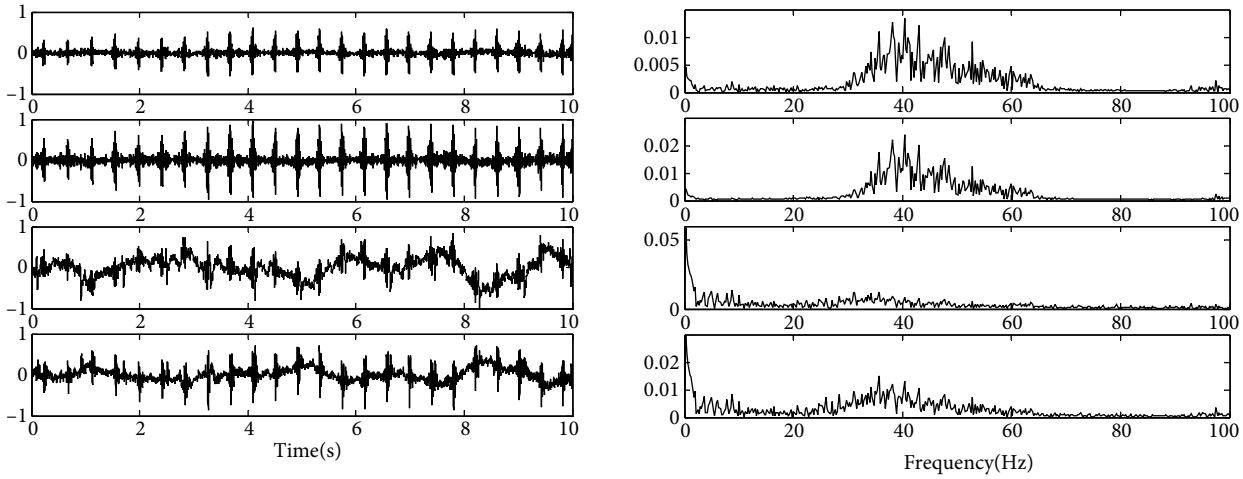

Figure 11. a) FECG estimates, $\underline{\hat{f}}(z)$, from Eq. (20), for the abdominal ECG dataset "a15" of Figure 7 by the proposed algorithm; b) spectra of the FECG estimates.

The results from applying the proposed algorithm to segments from the "a40" and "b08" abdominal ECG recordings in Figures 8 and 9, respectively, are shown in the 4th graph (from the top) of Figures 13a and 13b. For both of these datasets, the 1st output from SBR2C is back projected. These two datasets were also processed by the SBR2-based method, PiCA, and classical SVD method; the output signal from each method with the most visible FECG contributions is presented, respectively, in the 1st, 2nd, and 3rd sets of graphs of Figure 13. In Figure 13a, the actual fetal R-wave locations (obtained from the reference annotations) are indicated by downward-pointing arrows. The fetal heart rate is 144 bpm and the maternal heart rate is ~ 77 bpm. In the FECG estimate produced by our method, the fetal R-waves can be seen to coincide with the actual ones, with a few failures, indicated by upward-pointing arrows. Conversely, fetal components in the PCA, PiCA, and SBR2-based method are not so clear.

Experiments using other datasets from the PhysioNet database were repeated. For lack of space, all experimental results obtained from our investigation cannot be shown; however, about 65% of the results observed were similar to the examples shown here.

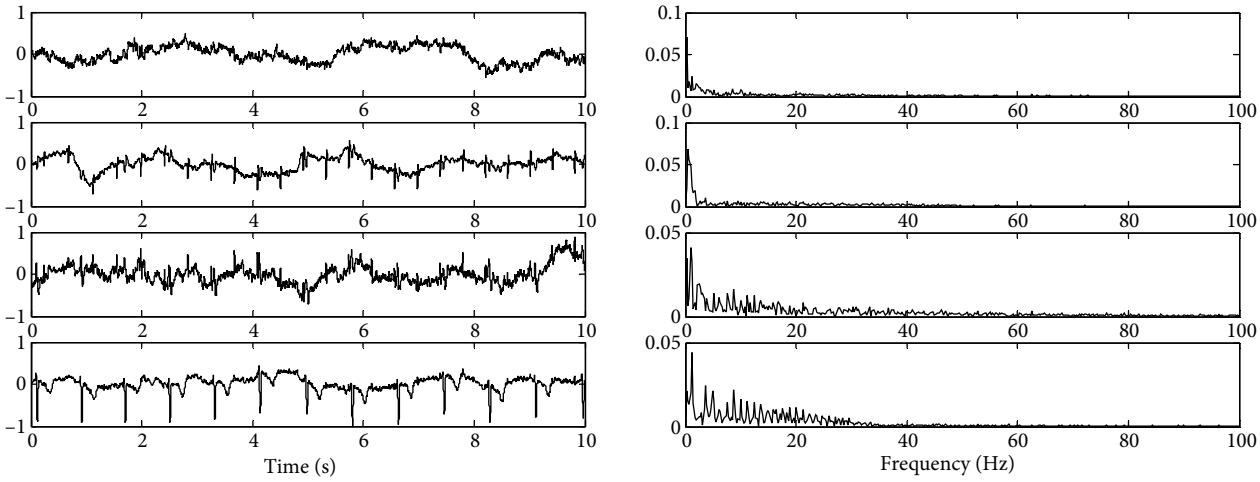

Figure 12. a) Periodic components extracted from the abdominal ECG dataset "a15" of Figure 7 using the PiCA; b) spectra of the PiCA estimates.

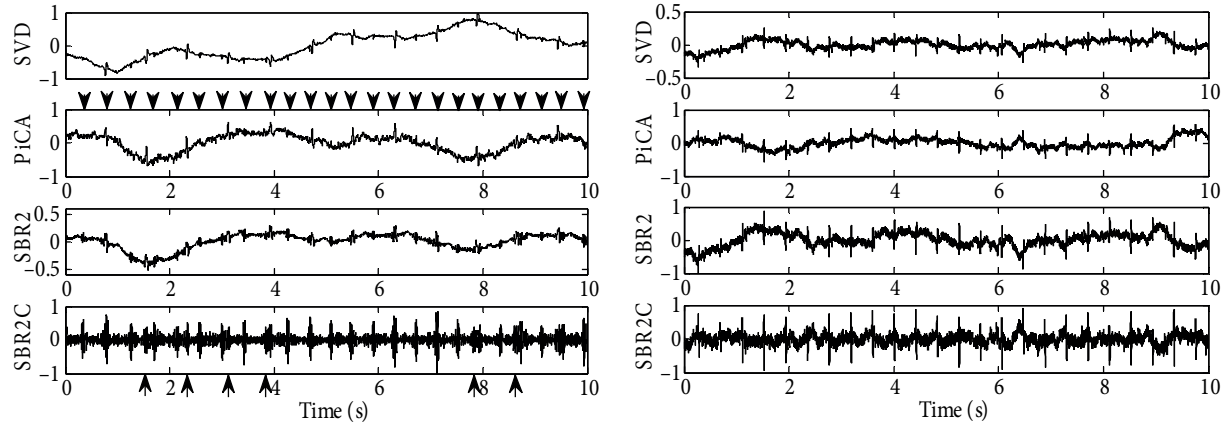

Figure 13. Comparison of the various methods for dataset a) "a40" of Figure 8 and b) "b08" of Figure 9: (from top to bottom) the first output from the SVD, PiCA, SBR2-based method, and our method.

5. Conclusion

In this paper, we have established a method that uses broadband subspace decomposition for the estimation of fetal ECG signals from multiple ECG abdominal recordings. Our method is based on a model that accounts for the effective broadband sensor array processor that manifests as a consequence of the broadband noise impinging on the sensors. Experiments with synthetic and real ECG data suggest that the proposed method works reasonably well.

Real-life experiments were conducted for the PhysioNet Challenge 2013 database, which is a difficult database because the fetal ECG signals are corrupted by the maternal ECG and broadband noises. The proposed scheme has shown overall success in extracting the fetal ECG signal for most of the tested datasets. Although the P- and T-waves were usually not discernable from the estimates provided by any of the methods tested, the proposed method is able to estimate the fetal R-waves with good accuracy.

The proposed method has been shown to give improved accuracy and robustness as compared to the prior-art. Our technique does not require preprocessing or postprocessing stages. Experiments indicate that its

sensitivity to sensor placement is low. The method also does not require measurement of the maternal ECG as a reference signal.

Future work consists of enhancing the automated back projection scheme with the development of an adaptive R-wave detection technique, which would make the method more practicable. Efforts will also focus on hardware implementation of the proposed algorithm, possibly on a field-programmable gate array, which would significantly improve execution times.

Acknowledgments

The author would like to thank Prof JG McWhirter of Cardiff University and Dr S Weiss of the University of Strathclyde for a number of very helpful discussions.

References

[1] Widmark C, Jansson T, Lindecrantz K, Rosen K. ECG waveform, short term heart rate variability & plasma catecholamine concentrations in response to hypoxia in intrauterine growth related guinea-pig fetuses. J Develop Physio 1991; 15: 161-168.

[2] Solum T, Ingermarson I Nygren A. The accuracy of abdominal ECG for fetal electronic monitoring. J Perinatal Med 1980; 8: 142-149.

[3] Assaleh K, Al-Nashash H. A novel technique for the extraction of fetal ECG using polynomial networks. IEEE T Biomed Eng 2005; 52: 1148-1152.

[4] Camps G, Martinez M, Soria E. Fetal ECG extraction using an FIR neural network. In: Proceedings of Computers in Cardiology; 2001. pp. 249-252.

[5] Sameni R, Shamsollahi MB, Jutten C, Clifford GD. A nonlinear Bayesian filtering framework for ECG denoising. IEEE T Biomed Eng 2007; 54: 2172-2185.

[6] Ferrara ER, Widrow B. Fetal electrocardiogram enhancement by time sequenced adaptive filtering. IEEE T Biomed Eng 1982; 29: 458-460.

[7] Wei Z, Hongxing L, Aijun H, Xinbao N, Jianchun C. Single-lead fetal electrocardiogram estimation by means of combining R-peak detection, resampling and comb filter. Med Eng Phy 2010; 32: 708-719.

[8] Zarzoso V, Nandi AK. Noninvasive fetal electrocardiogram extraction: blind separation versus adaptive noise cancellation. IEEE T Biomed Eng 2001; 48: 12-18.

[9] De Lathauwer L, De Moor B, Vandewalle J. Fetal electrocardiogram extraction by blind source subspace separation. IEEE T Biomed Eng 2000; 47: 567-572.

[10] Salustri C, Barbati G, Porcaro C. Fetal magnetocardiographic signals extracted by 'signal subspace' blind source separation. IEEE T Biomed Eng 2005; 52: 1140-1142.

[11] Sameni R, Jutten C, Shamsollahi MB. Multichannel electrocardiogram decomposition using periodic component analysis. IEEE T Biomed Eng 2008; 55: 1935-1940.

[12] Golub GH, Van Loan CF. Matrix Computations. 3rd ed. Baltimore, MD, USA: Johns Hopkins University Press; 1996.

[13] Clifford GD. Singular value decomposition and independent component analysis for blind signal separation. Bio Signal Image Process 2005; 44: 489-499.

[14] Cardoso JF, Souloumiac A. Blind beamforming for non-Gaussian signals. Inst Elect Eng Proc F Radar Sig Process 1993; 140: 362-370.

[15] Callaerts D, De Moor B, Vandewalle J, Sansen W, Vantrappen G, Janssens J. Comparison of SVD methods to extract the foetal electrocardiogram from cutaneous electrode signals. Med Bio Eng Comput 1990; 28: 217-224.

[16] Kanjilal PP, Palit S, Saha G. Fetal ECG extraction from single channel maternal ECG using singular value decomposition. IEEE T Biomed Eng 1997; 44: 51-59.

[17] Sameni R, Clifford GD, Jutten C, Shamsollahi MB. Multichannel ECG and noise modeling: application to maternal and fetal ECG signals. EURASIP J Adv Sig Process 2007; 2007: 43407.

[18] Sameni R, Clifford GD. A review of fetal ECG signal processing; issues and promising directions. Open Pacing Electrophysiol Ther J 2010; 3: 4-20.

[19] Micó P, Mora M, Cuesta-Frau D, Aboy M. Automatic segmentation of long-term ECG signals corrupted with broadband noise based on sample entropy. Comput Methods Programs Biomed 2010; 98: 118-129.

[20] Vaidyanathan PP. Theory of optimal orthonormal subband coders. IEEE T Sig Process 1998; 46: 1528-1543.

[21] Vaidyanathan PP. Multirate Systems and Filter Banks. Englewood Cliffs, NJ, USA: Prentice Hall; 1993.

[22] Lambert RH, Joho M, Mathis H. Polynomial singular values for number of wideband source estimation and principal components analysis. In: International Conference on Independent Component Analysis and Blind Signal Separation; 2001. pp. 379-383.

[23] McWhirter JG, Baxter PD, Cooper T, Redif S, Foster J. An EVD algorithm for para-Hermitian polynomial matrices. IEEE T Sig Process 2007; 55: 2158-2169.

[24] McWhirter JG. An algorithm for polynomial matrix SVD based on generalised Kogbetliantz transformations. In: Proceedings of the European Signal Processing Conference; 2010. pp. 457-461.

[25] Tkacenko A. Approximate eigenvalue decomposition of para-Hermitian systems through successive FIR paraunitary transformations. In: Proceedings of the IEEE International Conference on Acoustic Speech Signal Processing; 2010. pp. 4074-4077.

[26] Redif S, McWhirter JG, Weiss S. Design of FIR paraunitary filter banks for subband coding using a polynomial eigenvalue decomposition. IEEE T Sig Process 2011; 59: 5253-5264.

[27] Redif S, Fahrioglu U. Foetal ECG extraction using broadband signal subspace decomposition. In: IEEE Mediterranean Microwave Symposium; 2010. pp. 381-384.

[28] Liu GS, Wei CH. A new variable fractional sample delay filter with nonlinear interpolation. IEEE T Circuits-II 1992; 39: 123-126.

[29] Kailath T. Linear Systems. Englewood Cliffs, NJ, USA: Prentice Hall; 1980.

[30] Goldberger AL, Amaral LAN, Glass L, Hausdorff JM, Ivanov PC, Mark RG, Mietus JE, Moody GB, Peng CK, Stanley HE. PhysioBank, PhysioToolkit, and PhysioNet: Components of a new research resource for complex physiologic signals. Circulation 2000; 101: e215-e220.

[31] Moody GB, Mark RG. The impact of the MIT-BIH Arrhythmia Database. IEEE Eng Med Biol 2001; 20: 45-50.

[32] Moody GB, Mark RG, Goldberger AL. PhysioNet: A web-based resource for the study of physiological signals. IEEE Eng Med Biol 2001; 20: 70-75.